Time-Resolved X-ray Absorption Determination of Structural Changes following Photoinduced Electron Transfer within Bis-porphyrin Heme Protein Models

Lin X. Chen,*,† Peter L. Lee,‡ David Gosztola,† Walter A. Svec,† Pedro A. Montano,§ and Michael R. Wasielewski*,†,||

Chemistry Division, Experimental Facilities Division and Materials Science Division, Argonne National Laboratory, Argonne, Illinois 60439-4831, and Department of Chemistry, Northwestern University, Evanston, Illinois 60208-3113

Received: January 5, 1999

Time domain energy dispersive X-ray absorption spectroscopy provides a powerful probe of changes in molecular structure that occur during photoinduced electron transfer reactions. In this study a diporphyrin model for electron transfer within modified heme proteins is examined using this technique. Transient optical absorption experiments show that photoinduced electron transfer from the lowest excited triplet state of a Zn porphyrin attached at a fixed 25 Å distance by means of a long spacer molecule to an Fe(III) porphyrin occurs with a 6 ms time constant at 77 K. Time domain X-ray absorption measurements are consistent with transient reduction of Fe(III) to Fe(II) that is accompanied by substantial weakening of the bond between the Fe atom and a pyridine molecule ligated to it. Coupling of ligand loss to reduction of Fe(III) to Fe(II) provides a means of stabilizing the reduced intermediate.

Introduction

Photoinduced electron transfer (ET) reactions are important in many biological and chemical systems. The rates of these reactions depend critically on the coupling of the electron motion to nuclear motions within the electron donor and acceptor molecules as well as to those of molecules in the surrounding environment.[1] Most photoinduced ET reactions result in the formation of intermediates that are too short-lived for conventional X-ray structure determination. In principle, time-resolved X-ray techniques can be used to determine the structural changes that occur during ET reactions, yet many of these techniques have become technically feasible only recently.[2,3] Although photodissociation of CO from the heme cofactor within carbonmonoxymyoglobin was studied using time-resolved X-ray absorption techniques more than a decade ago,[4] structural data on species that result from photoinduced ET have only been obtained for intermediates that can be matrix isolated at low temperatures and studied with steady-state X-ray methods.[5,9]

Photoinduced ET reactions have been studied extensively in a variety of modified heme proteins,[10−14] including hybrid hemoglobins in which one Fe(III) porphyrin (Fe(III)P) is replaced by a Zn or Mg porphyrin (ZnP or MgP).[15−17] Photoexcitation of ZnP or MgP produces the lowest excited triplet state, ^{3}ZnP or ^{3}MgP, respectively, which donates an electron to a distant Fe(III)P.[15−17] Many of these photoinduced ET reactions in heme proteins occur on a millisecond time scale.[15−17] In this study time domain energy dispersive X-ray absorption spectroscopy (EDXAS)[18−20] with 5 ms time resolution is used to directly probe structural changes that occur in the biomimetic model compound **2** (Figure 1), when it undergoes the photoinitiated ET reaction

$$^3\mathrm{ZnP}-\mathrm{L}-\text{spacer}-\mathrm{Fe(III)P}-\mathrm{L} \rightarrow \mathrm{ZnP}^+-\mathrm{L}-\text{spacer}-\mathrm{Fe(II)P}-\mathrm{L} \quad (1)$$

where ligand L = acetate (AcO^-) or pyridine (py). Compound **1**, which does not have an electron acceptor, Fe(III)P−L, is used as a reference compound. The Zn−Fe distance in **2** is 25 Å, which is comparable to that in the hybrid hemoglobins,[15−17] while that in compound **3** is 45 Å.[21]

Experimental Section

The syntheses of compounds **1**−**3** were carried out using variations of established procedures.[22] The structures of these compounds were completely characterized by proton NMR, mass spectral analysis, and UV−visible spectroscopy. 2-Methyltetrahydrofuran (Aldrich) was freshly distilled from lithium aluminum hydride immediately prior to use.

Cyclic voltammetry on **1**−**3** was carried out in a standard three-electrode cell using Pt working, Pt auxiliary, and saturated calomel reference electrodes (SCE) in 10^{-3} M solutions of **1**−**3** in butyronitrile containing 0.1 M tetra-*n*-butylammonium perchlorate. The resultant half-wave potentials for one-electron oxidation and reduction of **1**−**3** are discussed in the text.

Ground state optical absorption measurements were made with a Shimadzu UV160 spectrometer. Nanosecond transient optical absorption experiments were carried out using 425 nm, 4 ns, 1 mJ laser pulses from a frequency-tripled Continuum Surelite II Nd-YAG-Surelite OPO laser system. The laser-illuminated area at the sample is about 0.12 cm^2. The probe light was a cw tungsten lamp. The transient absorption signal was collected using a Hamamatsu R928 PMT at a wavelength selected by a monochromator (H-20, Instrument SA, Inc.) with a band width of 2 nm. The transient absorption decay traces were captured by a digital oscilloscope (HP 54522A) with background correction. Typical decay time ranges monitored were 20−100 ms. Samples for the transient absorption experi-

* To whom correspondence should be addressed.
† Chemistry Division, Argonne National Laboratory.
‡ Experimental Facilities Division, Argonne National Laboratory.
§ Materials Science Division, Argonne National Laboratory.
|| Northwestern University.

10.1021/jp990056j CCC: $18.00
Published on Web 04/02/1999

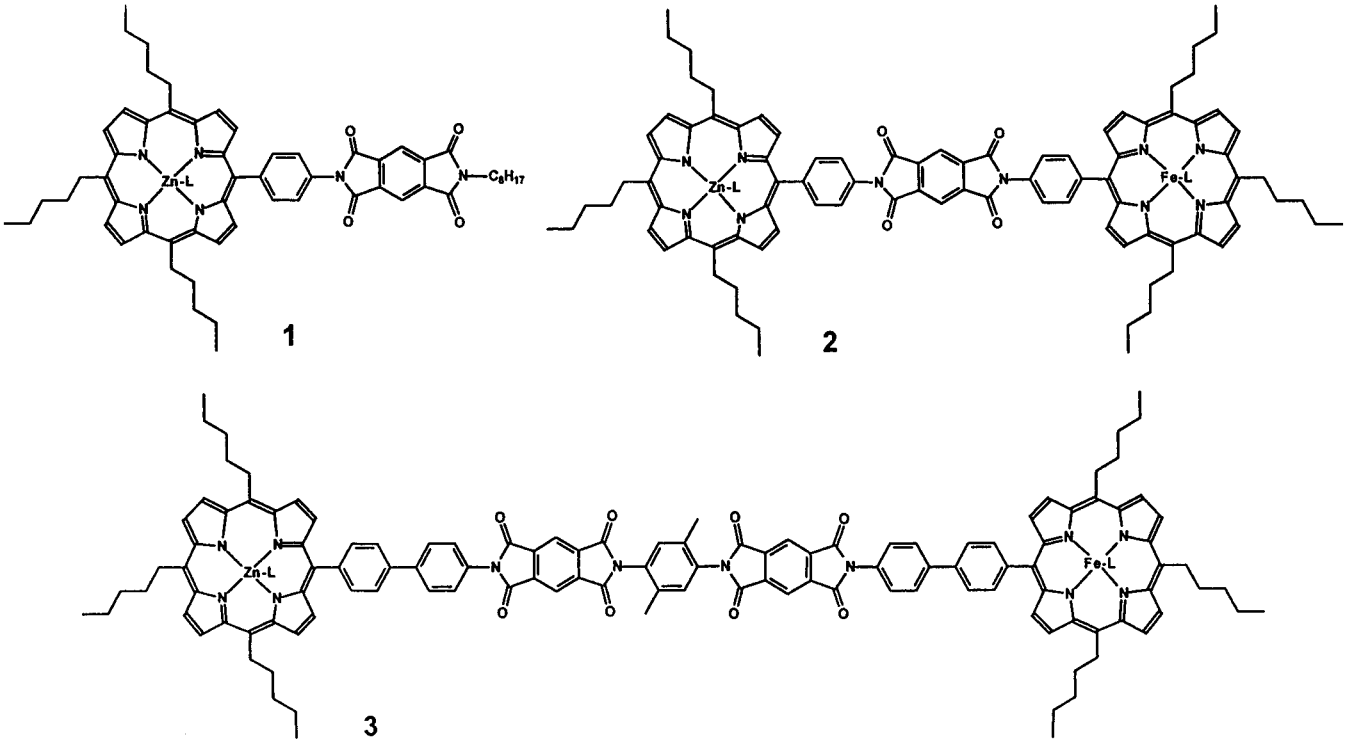

Figure 1. Molecular structures of **1**−**3**.

ments had optical densities for 1-mm pathlength cells of ∼0.5 (concentration < 10^{-5} M) and were freeze−pump−thaw degassed three times prior to cooling to 77 K in an immersion dewar. Femtosecond transient optical absorption experiments were carried out using apparatus and techniques described elsewhere.[23]

EDXAS measurements were carried out at the beamline X6A, National Synchrotron Light Source (NSLS), Brookhaven National Laboratory. The configuration of the beamline has been described elsewhere.[18] A bent Si(220) crystal was used as a polychromator, which diffracted and focused the synchrotron beam horizontally to a 0.2 mm spot at the sample. The vertical beam size was defined by slits at 0.8 mm. The divergent beam of X-rays from the synchrotron is diffracted with a slightly different energy at each point. This creates a continuous energy spectrum horizontally. A linear photodiode array detector with 1024 pixels and 25 μm pixel size was used to collect the whole energy spectrum simultaneously. The time resolution of the EDXAS apparatus is 5 ms, which is limited primarily by the detector read-out time.[18] The spectra were calculated using $\log[(I_{\text{reference}} - I_{\text{dark}})/(I_{\text{sample}} - I_{\text{dark}})]$, where $I_{\text{reference}}$, I_{dark}, and I_{sample} are the transmitted X-ray intensities detected by the diode array through the blank solvent, with X-ray shutter closed, and through the sample, respectively, with the same integration time. Photoexcitation of ZnP at 563 nm was provided by laser pulses from a Nd:YAG pumped OPO system (Spectra Physics, GCR170-10 and MOPO 710) at a 10 Hz repetition rate using 30 mJ pulses. The laser pulses were synchronized to the detector read-out. The absorption coefficient for visible light of a 2 mM solution of **2** at 563 nm is about 2000 times larger than that for X-ray photons near the Fe K-edge at 7.1 keV. To compensate for this difference, a special cell geometry for the sample was adopted, which allows efficient visible photoexcitation of the sample and yields reasonable signal-to-noise ratios of XAS spectra with transmission detection in EDXAS. A copper sample cell with two identical compartments was constructed with two parallel Mylar windows for X-ray transmission, one for the blank solvent as the reference, and the other for the sample. The cell had a quartz window for laser beam transmission sealed at a right angle with respect to the Mylar windows. The X-ray beam is able to pass through 3-mm of the frozen solution sample at a point very close (e.g., 0.3 mm) to the inner surface of the quartz window. This configuration provides a factor of 10 compensation for the discrepancy between the visible light and X-ray absorption coefficients. This design enables measurements in the XANES (X-ray absorption near edge structure) region at 7.1 KeV for a sample with only 2 mM concentration using a transmission geometry. The energies of the EDXAS spectra were calibrated by the standard metal foil spectrum collected with the same detector. The sample was freeze−pump−thaw degassed and was under vacuum during the experiment. The sample cell was mounted on the cold tip of a Helitran cryogenic system (Air Products), and the temperature of the cold tip was maintained at 70 K. The experiments were repeated four times to ensure that the observed spectral changes are reproducible. During the entire data acquisition process, the Fe K-edge position remained unchanged within the resolution of each pixel, 0.4 eV, in the linear diode array detector. Each data acquisition cycle includes 20 s of integration time for the dark, the solvent reference, and the sample, and then 10 cycles are included in each data set. The trigger for the linear diode array read-out is synchronized with the laser and detector read out 10 times between two laser pulses (100 ms time interval). Therefore, each data set is the result of 200 s of accumulated integration time.

Results and Discussion

Electron Transfer Energetics. At room temperature, $\Delta G°$ for the reaction ^{1}ZnP−L−spacer−Fe(III)P−L or ^{3}ZnP−L−spacer−Fe(III)P−L → ZnP$^+$−L−spacer−Fe(II)P−L in **2** and **3** depends on the ligand L coordinated to the Fe. These free energies of reaction were calculated using

$$\Delta G° = E_{\text{OX}} - E_{\text{RED}} - e_0^2/(\epsilon_S R_{\text{DA}}) - E_S \qquad (2)$$

TABLE 1: Time Constants for ZnP Triplet State Decay and Ground State Recovery at 77 K

compound	τ (ms) at 475 nm	τ (ms) at 560 nm
ZnP (AcO^- or py)	20.3 ± 0.1	16.7 ± 0.1
1 + AcO^- or py	18.3 ± 0.1	17.7 ± 0.1
2 + AcO^-	17.8 ± 0.5	15.8 ± 0.2
2 + Py	5.6 ± 0.1	7.9 ± 0.2
3 + AcO^-	15.9 ± 0.1	14.2 ± 0.5
3 + Py	15.5 ± 0.1	19.0 ± 0.7

where E_S is the 2.05 eV lowest excited singlet state energy of ZnP, E_{OX} and E_{RED} are the one-electron oxidation and reduction potentials of ZnP−L, where L = AcO^- and py (0.62 V vs SCE), Fe(III)P−OAc (−0.5 V vs SCE), and Fe(III)P−py (0.0 V vs SCE), respectively, measured in butyronitrile, R_{DA} is donor−acceptor center-to-center distance, ϵ_S is the static dielectric constant of the solvent and e_0 is the electronic charge. Using eq 2 at room temperature, $\Delta G°$ for ET from ^{1}ZnP−L and ^{3}ZnP−L to the pyromellitimide (PI) within the spacer is −0.6 eV and −0.2 eV, respectively. In both **2** and **3**, if L = AcO^-, $\Delta G° = -0.9$ eV and −0.5 eV, respectively, for ET from ^{1}ZnP−L or ^{3}ZnP−L to Fe(III)P−L, while if L = py, $\Delta G° = -1.4$ eV and −1.0 eV, respectively. The experiments are carried out in a 2-methyltetrahydrofuran (MTHF) glass at 77 K to prevent ET from ^{1}ZnP−L or ^{3}ZnP−L to the PI spacer. It has been shown previously that $\Delta G°$ for ET reactions using porphyrin donors is approximately 0.8 eV more positive in glassy MTHF at 77 K than in the polar organic solvents in which the electrochemical redox data are obtained.[24] Therefore, the rates of the ET reactions from ^{1}ZnP−L or ^{3}ZnP−L to PI at 77 K are very slow relative to the excited state decay rates of ^{1}ZnP−L or ^{3}ZnP−L because $\Delta G° = 0.2$ and 0.6, respectively. At 77 K, for ET from ^{1}ZnP−L or ^{3}ZnP−L to Fe(III)P−OAc, $\Delta G° \cong -0.1$ and 0.3, respectively, while for ET from ^{1}ZnP−L or ^{3}ZnP−L to Fe(III)P−py, $\Delta G° \cong -0.6$ and −0.2, respectively. Given the long 25 and 45 Å donor−acceptor distances within **2** and **3**, respectively, as well as the short, 2 ns lifetime of ^{1}ZnP−L, ET from ^{1}ZnP−L to Fe(III)P−L should be inefficient, regardless of the free energy of reaction. On the other hand, given the long, 20 ms lifetime of the ^{3}ZnP−L state, ET across relatively long distances should occur, if the free energy of the ET reaction is sufficiently negative. The free energy data given above suggest that ET from ^{3}ZnP−L to Fe(III)P−py should occur, while that from ^{3}ZnP−L to Fe(III)P−OAc should not occur.

Transient Optical Spectroscopy. To verify the occurrence of the photoinduced ET processes and to establish the rate constants for the reactions in **1**−**3**, a series of optical transient absorption measurements were performed. Transient optical absorption spectra of **1**−**3** at 77 K were measured as a function of time after photoexcitation using 425 nm, 4 ns, 1 mJ laser pulses. The concentration of ^{3}ZnP was monitored at 475 nm,[25] while the ground-state recovery kinetics were monitored at 560 nm. The 425 nm laser pulses excite both Zn−P and Fe(III)P. However, the excited states of Fe(III)P decay to ground state with time constants of about 15 ps[26] and are not involved in the slow electron transfer processes monitored in **2**. The time constants for triplet state decay and ground-state recovery at 77 K are listed in Table 1. In addition, Figure 2 shows the transient absorption kinetics for **2** at 475 and 560 nm. At 77 K, ZnP and **1** have triplet state decay time constants of about 18−20 ms. Compounds **2** and **3** with acetate ligands on Zn and Fe exhibit almost the same decay time constants, 16−18 ms. However, adding pyridine ligands to each of the metals in **2** shortens the decay time constant of ^{3}ZnP within **2** to 6 ms, while those in **1** and **3** remain unchanged. The ground-state recovery time constants display the same trends, where only **2** with pyridine ligands showed a shortened time constant of 8 ms compared to 14−19 ms for the other molecules studied. The shortened time constants of ^{3}ZnP within **2** with pyridine ligands suggest that a new triplet-quenching mechanism occurs when **2** is ligated with pyridine.

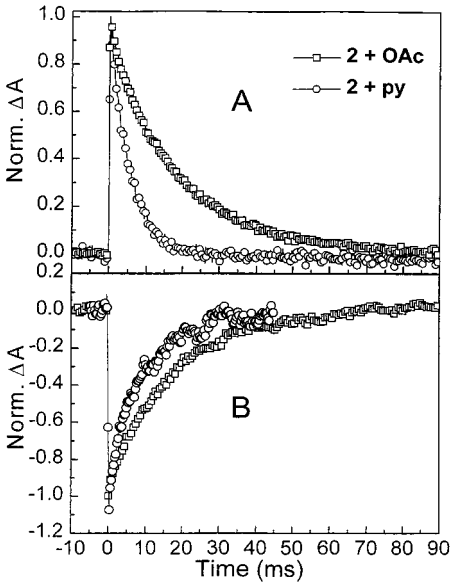

Figure 2. Transient optical absorption kinetics for **2** with the indicated ligands at 77 K following 425 nm excitation (A) monitored at 475 nm and (B) monitored at 560 nm.

Three possible quenching mechanisms for ^{3}ZnP−py in **2** were considered: (a) ET from ^{3}ZnP−py to Fe(III)−py, forming ZnP^+−py and Fe(II)P−py; (b) energy transfer from ^{3}ZnP−py to Fe(III)P−py, and (c) quenching of ^{3}ZnP in ^{3}ZnP−py by the pyridine ligand. Possibility c was eliminated because the triplet-state decay kinetics of **3** (with a donor−acceptor distance of 45 Å) were unchanged by ligation of Fe and Zn with pyridine. The triplet decay time constants for **2** and **3** with acetate ligands on the metals are almost the same as that for **1**, which suggests that energy transfer from ^{3}ZnP to Fe(III)P is very inefficient and does not contribute appreciably to the decay of ^{3}ZnP. Ligation of Fe(III)P with pyridine in both **2** and **3** makes the free energy of reaction for ET more favorable by about 0.5 eV. The fact that quenching of ^{3}ZnP−py occurs only in **2** suggests that path a is the most plausible quenching mechanism. Adding a pyridine ligand to the Fe in **3** does not affect the triplet state decay rate in **3**, because the longer donor−acceptor distance in **3** decreases the electronic coupling between them. Thus, ET in **3** does not occur even though $\Delta G°$ for this reaction is favorable. All the optical results taken together strongly suggest that the quenching of ^{3}ZnP when pyridine ligates Zn and Fe in 2 is due to ET from ^{3}ZnP−py to Fe(III)P−py with a 6 ms time constant. Since the ground-state recovery data indicates that back-ET occurs with an 8 ms time constant, the lifetime of the transient Fe(II)P−py intermediate is long enough to accumulate a sufficient concentration of charge separation intermediate, ZnP^+−L−spacer−Fe(II)P−py, for detection in the EDXAS experiment, which allows us to probe the molecular structure in the vicinity of its Fe atom.

Transient X-ray Absorption Spectroscopy. Because the optical transient absorption measurements show that the photoinduced ET reaction in eq 1 occurs in **2**, oxidation state as well as geometry changes around the Fe atom in **2** can contribute

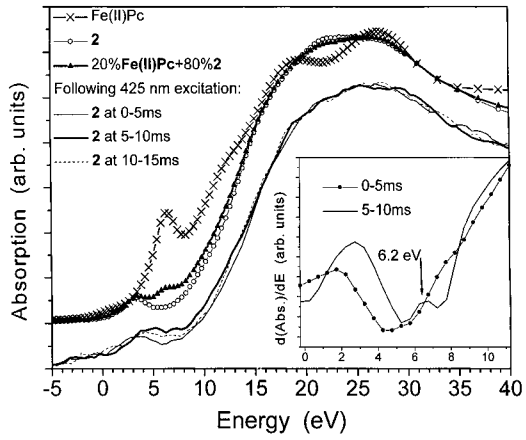

Figure 3. XANES spectra of Fe(II)Pc, the ground state of **2**, a linear combination of 20% Fe(II)Pc and 80% ground state **2**, and **2** at different detection times after the laser pulse. The inset shows the smoothed first derivative of the XANES spectrum of **2** at two different times. The appearance of a structure similar to that of Fe(II)Pc is evidenced by the peak at 6.2 eV.

to the transient XANES spectra. The effects of the oxidation and coordination states of the Fe atom in porphyrin-like structures on their XANES spectra can be demonstrated by comparing the XANES spectra of the Fe(II) phthalocyanine (Fe(II)Pc) ground state with that of **2** taken at a conventional XAFS beamline (X6B, NSLS), shown in Figure 3. The Fe(II) within Fe(II)Pc has a square planar geometry,[27] while the Fe(III) within **2** has a square pyramidal geometry. These oxidation state and coordination geometry changes result in the following differences between the XANES spectra: (1) the transition edge energy for Fe(II)Pc in the 8−15 eV region moves to lower energy relative to that of **2**, (2) a sharp peak appears in the middle of the rising transition edge for Fe(II)Pc at ∼6.2 eV, and (3) the small pre-edge peak for ground state **2** at 3 eV is not present in Fe(II)Pc. The first change is due to the lower positive charge on the Fe atom in the Fe(II) complex relative to that of the Fe(III) complex. This results in a lower energy requirement for excitation of the 1s electron to the continuum in the Fe(II) complex relative to that for the Fe(III) complex. The second change results from a transition from the 1s orbital to an orbital with p_z character, most likely, $4p_z$,[28] based on the X-ray polarization dependence of XAFS spectra in $CuC1_4^{2-}$ and carbonmonoxymyoglobin.[28,29] The third change is due to the molecular symmetry difference between the centrosymmetric square planar and noncentrosymmetric pyramidal square geometries. The pre-edge peak at 3 eV arises from a symmetry forbidden transition 1s → 3d. For a centrosymmetric geometry, this feature is very weak and is only quadrupole allowed, such as in square planar Fe(II)Pc (Figure 3) and octahedral Fe(II)-$PcPy_2$ (not shown) geometries. When the 3d orbital is mixed with the 4p orbital in a noncentrosymmetric geometry, such as a square pyramid, the 1s → 3d transition becomes slightly allowed,[30] resulting in an increase in the pre-edge peak seen at 3 eV in the spectrum of ground state **2**.

XANES spectra taken at the EDXAS beamline for **2** at the Fe K-edge (7.112 keV) at different time delays following the laser excitation pulse are also shown in Figure 3. The spectrum of **2** obtained at 0−5 ms following laser excitation is very similar to that of its ground state because at these early times the population of photoreduction product is very low. The largest changes in the XANES spectrum of **2** occur 5−10 ms following laser excitation, when the spectrum shows an apparent increase in the pre-edge feature in the 3−8 eV region and a slight downshift of the transition energy at the beginning of the transition edge in the 8−15 eV region. Moreover, the positions of the pre-edge features appear shifted to an energy 2−2.5 eV higher than those of the ground state. At 10−15 ms following laser excitation, the changes observed at 5−10 ms relax back to the XANES spectral features observed for ground state **2**.

While the transient optical absorption results show that photoreduction of Fe(III) to Fe(II) in **2** occurs, the visible light optical experiment does not address the nature of the structural changes that may accompany this oxidation state change. Ligand coordination changes as well as oxidation state changes are reflected in the XANES spectra. Ligand coordination around the Fe(III) can be either unchanged, reduced to a four-coordinate square planar, or increased to a six-coordinate octahedral geometry. Moreover, Fe−ligand distance changes could also accompany the reduction of Fe(III). The Fe K-edge XANES spectrum of **2** at 5−10 ms shown in Figure 3 consists of the spectrum of the ground state mixed with that of Fe(II) within the ZnP^+−L−spacer−Fe(II)P−py intermediate generated by the laser pulse. After careful examination of several Fe-containing porphyrin and phthalocyanine complexes with different coordination geometries, oxidation states, and the nearest neighbor distances, this spectrum can be best fit by a linear combination of 20% of the spectrum due to Fe(II)Pc and 80% of that due to the ground state of **2**. This linear combination spectrum, shown in Figure 3 (▲), was computed from the measured spectra of Fe(II)Pc and ground state **2**. The down-shift of the edge energy in the region of 8−15 eV in the spectrum of **2** at 5−10 ms following laser excitation from that of **2** at 0−5 ms is comparable to the down-shift of the edge in the mixed spectrum from that of the ground-state spectrum of **2**. The inset to Figure 3 shows the first derivative of the spectrum of **2** at 5−10 ms following laser excitation. The derivative shows an inflection at 6.2 eV, where the sharp peak in the XANES spectrum of square planar Fe(II)Pc occurs. Because of the low sample concentration (∼2 mM), a structural analysis using the EXAFS region is not feasible using the transmission detection geometry in EDXAS. However, the spectral changes from the XANES region verify the electronic structural changes due to photoreduction and suggest a geometry where the bond between the pyridine ligand and the Fe in the intermediate ZnP^+−py−spacer−Fe(II)P−py has been broken or substantially weakened.

Conclusions

Evidence for the square planar geometry around the Fe atom in the ZnP^+−py−spacer−Fe(II)P−py intermediate indicates that the ligand may serve to gate the ET. When pyridine binds to Fe(III), $\Delta G°$ for reduction to Fe(II) is more favorable. However, once the electron is transferred to Fe(III)P−py, breaking the Fe−pyridine bond makes $\Delta G°$ for back-electron-transfer to the ground state more negative. Since the energy gap between the ET intermediate and the ground state is most likely in the Marcus inverted region,[31] the larger energy gap due to loss of the pyridine ligand in the intermediate results in a slower back-electron-transfer rate. Thus, the combined optical and X-ray results indicate that pyridine ligation enables ET both into and out of the iron porphyrin, while dissociation of the ligand hinders these processes. Time-resolved X-ray structural studies combined with transient optical studies provide a powerful tool for elucidating the mechanisms of ET reactions. Application of these techniques to both biological and chemical ET events on a time scale approaching 100 ps will be possible in the very near future using apparatus currently being assembled at the Advanced Photon Source at the Argonne National Laboratory.

Acknowledgment. This work was supported by the Division of Chemical Sciences, Office of Basic Energy Sciences, Department of Energy under contract W-31-109-ENG-38. The authors would like to thank Dr. Guy Jennings for his help in data acquisition programs.

References and Notes

(1) Barbara, P. F.; Meyer, T. J., Ratner, M. A. *J Phys. Chem.* **1996**, *100*, 13148.

(2) Perman, B.; Srajer, V.; Ren, Z.; Teng, T-Y.; Pradervand, C.; Ursby, T.; Bourgeois, D.; Schotte, F.; Wulff, M.; Kort, R.; Hellingwerf, K; Moffat, K. *Science* **1998**, *279*, 1946.

(3) Thiel, D. J.; Livins, P.; Stem, E. A.; Lewis, A. *Nature* 1993, *363*, *565*.

(4) Mills, D. M.; Lewis, A.; Harootunian, A.; Huang, J.; Smith, B. *Science* **1984**, *223*, 811.

(5) Chance, B.; Fischetti, R.; Powers, L. *Biochemistry* **1983**, *22*, 3820.

(6) Powers, L.; Sessler, J. L.; Woolery, G. L.; Chance, B. *Biochemistry 1984*, *23*, *5519*.

(7) Chen, L. X.; Bowman, M. K.; Montano, P. A.; Norris, J. R. *J. Am. Chem. Soc.* **1993**, *115*, 5519.

(8) Chen, L. X.; Bowman, M. K.; Wang, Z.; Montano, P. A.; Norris, J. R. *J. Phys. Chem.* **1994**, *98*, 9467.

(9) Chen, L. X.; Wang, Z.; Burdett, J. K.; Montano, P. A.; Norris, J. R. *J. Phys. Chem.* **1995**, *99*, 7958.

(10) Di Bilio, A. J.; Hill, M. G.; Bonander, N.; Karlsson, B. G.; Villahermosa, R. M.; Malmstroem, B. G.; Winkler, J. R.; Gray, H. B. *J. Am. Chem. Soc.* **1997**, *119*, 9921.

(11) Gray, H. B.; Winkler, J. R. *Annu. Rev. Biochem.* **1996**, *65*, 537.

(12) Wishart, J. F.; Sun, J.; Cho, M.; Su, C.; Isied, S. S. *J. Phys. Chem.* **1997**, *B 101*, 687.

(13) Hake, R.; Corin, A.; McLendon, G. *J. Am. Chem. Soc.* **1997**, *119*, 10557.

(14) McLendon, G. *Bioinorg. Chem.* **1995**, *1*, 317.

(15) Nocek, J. M.; Sishta, B. P.; Casey, J. R.; Mauk, A. G.; Hoffman, B. M. *J. Am. Chem. Soc.* **1997**, *119*, 2146.

(16) Natan, M. J.; Baxter, W. W.; Kuila, D.; Gingrich, D. J.; Martin, G. S.; Hoffman, B. M. *Adv. Chem. Ser.* **1991**, *228*, 201.

(17) McGourty, J. L.; Blough, N. V.; Hoffman, B. M. *J. Am. Chem. Soc.* **1983**, *105*, 4470.

(18) Fontaine, A.; Baudelet, F.; Dartyge, E.; Guay, D.; Itie, J. P.; Polian, A.; Tolentino, H.; Tourillon, G. *Rev. Sci. Instrum.* **1992**, *63*, 960.

(19) Lee, P. L.; Beno, M. A.; Jennings, G.; Ramanathan, M.; Knapp, G. S.; Huang, K.; Bai, T.; Montano, P. A. *Rev. Sci. Instrum.* **1996**, *65*, *1*.

(20) Tolentino, H.; Dartyge, E.; Fontain, A.; Tourillon, G. *J. Appl. Crystallogr.* **1988**, *21*, 15.

(21) Donor−acceptor center-to-center distances were determined from structures calculated using the MM+ force field in Hyperchem 5.01a (Hypercube, Waterloo, Ontario, Canada).

(22) Gosztola, D.; Niemczyk, M. P.; Wasielewski, M. R. *J. Am. Chem. Soc.* **1998**, *120*, 5118.

(23) Greenfield, S. R.; Svec, W. A.; Gosztola, D.; Wasielewski, M. R. *J. Am. Chem. Soc.* **1996**, *118*, 6767.

(24) Gaines, III, G. L.; O'Neil, M. P.; Svec, W. A.; Niemczyk, M. P.; Wasielewski, M. R. *J. Am. Chem. Soc.* **1991**, *113*, 719.

(25) Pekkarinen, L.; Linschitz, H. *J. Am. Chem. Soc.* **1960**, *82*, 2407.

(26) Cornelius, P. A.; Steele, A. W.; Chernoff, D. A.; Hochstrasser, R. M. *Chem. Phys. Lett.* **1981**, *82*, *9*.

(27) Coppens, P.; Li, L. *J. Chem. Phys.* **1984**, *81*, 1983.

(28) Smith, T. A.; Penner-Hahn, J. E.; Berdin, M. A.; Doniach, S.; Hodgson, K. O. *J. Am. Chem. Soc.* **1985**, *107*, *5945*.

(29) Bianconi, A.; Cogiu-Castellano, A.; Durham, P. J.; Hasnain, S. S.; Phillips, S. *Nature* **1985**, *318*, 685.

(30) Cartier, C.; Monenteau, M.; Dartyge, E.; Fontaine, A.; Tourillon, G.; Michalowicz, A.; Verdaguer, M. *J. Chem. Soc. Dalton Trans.* **1992**, 609.

(31) Marcus, R. A. *J. Chem. Phys.* **1956**, *24*, 966.